Nano Energy 48 (2018) 560–568

Contents lists available at ScienceDirect

Nano Energy

journal homepage: www.elsevier.com/locate/nanoen

Full paper

Atomic structure and migration dynamics of MoS_2/Li_xMoS_2 interface

Shulin Chen[a,b,1], Liping Wang[c,1], Ruiwen Shao[b], Jian Zou[c], Ran Cai[d], Jinhuang Lin[a], Chongyang Zhu[d], Jingmin Zhang[b], Feng Xu[d,*], Jian Cao[a], Jicai Feng[a], Junlei Qi[a,*], Peng Gao[a,b,e,f,**]

[a] State Key Laboratory of Advanced Welding and Joining, Harbin Institute of Technology, Harbin 150001, China
[b] Electron Microscopy Laboratory, School of Physics, Peking University, Beijing 100871, China
[c] School of Materials and Energy, State Key Laboratory of Electronic Thin Film and Integrated Devices, University of Electronic Science and Technology of China, Chengdu 610054, China
[d] SEU-FEI Nano-Pico Center, Key Laboratory of MEMS of the Ministry of Education, Southeast University, Nanjing 210096, China
[e] Collaborative Innovation Center of Quantum Matter, Beijing 100871, China
[f] International Center for Quantum Materials, School of Physics, Peking University, Beijing 100871, China

ARTICLE INFO

Keywords:
in situ TEM
2D materials
Lithium ion diffusivity
Phase transition
Phase interface
Aberration corrected STEM

ABSTRACT

The performance of alkali-metal-ion batteries largely depends on the migration behavior of alkali metal ions in the electrodes. Probing the atomic structure of the reaction interface and the dynamic process during ion transport in the electrodes will help better understand the underlying electrochemical mechanisms and inspire rational electrode designs. In this study, by combining *in situ* transmission electron microscopy (TEM) and aberration-corrected scanning TEM (STEM), we track the reversible lithium ion transport in MoS_2 nanostructures to reveal the atomic structure and dynamic behaviors of the reaction interface. We find that lithium ions insertion triggers complex phase transformations. Three different phases co-exist at the interface: a pristine 2H phase, a 1T phase with a shrank lattice constant of − 3.3% (± 2.3%), and a distorted 1T phase (called 1T′ phase) with an expanded lattice constant of 5.5% (± 2.5%). The atomically resolved Z-contrast image shows that the expanded 1T′ phase has distorted Mo arrangements. Furthermore, the lithium ions migration causes defects at the reaction front, and the diffusion on the surface is faster than that inside, forming a core-shell structure at the reaction interface. The diffusivity of lithium ions is directly measured to be ~1000–30,000 nm^2/s, which is significantly higher than that of sodium insertion (~10–20 nm^2/s). The atomic-scale observations of lithium-ion-migration-induced complex structural evolutions would help understand the properties of MoS_2 nanostructures and shed light on the design of alkali-metal-ion batteries with general transition-metal dichalcogenide electrodes.

1. Introduction

For decades, molybdenum disulfides (MoS_2) have been widely explored and employed as energy storage mediums [1–4]. MoS_2 crystal comprises hexagonally coordinated S-Mo-S′ atomic slabs bounded by weak van der Waals forces [5,6], structurally resembling graphite. The large space between two slabs can accommodate reversible alkali-metal-ion intercalation without significant volume expansion, making MoS_2 a promising candidate as an electrode material for batteries [7–10]. It is known complex structural changes occur during the migration of alkali metal ions in MoS_2. Previous studies have shown that the structural framework would deteriorate after the alkali-metal-ion intercalation in MoS_2 because of a transition from a pristine trigonal 2H phase into an octahedral 1T phase [11–13], induced by gliding atomic planes of sulphur [14]. The two phases (1T and 2H) exhibit different electronic structures, with the 2H phase being semiconducting and the 1T phase being metallic [15,16]. Consequently, the difference in the migration dynamics of alkali metal ions in MoS_2 is significant between them [17–19]. In fact, *in situ* X-ray diffraction (XRD) study has shown the existence of asymmetric phase transition pathways during the insertion and extraction of alkali-metal-ions in MoS_2, i.e., the phase transition from 2H MoS_2 to 1T Na_xMoS_2 is a two-phase reaction during Na ions insertion, whereas the phase transition from 1T to 2H during Na ions extraction is solid-solution-like [17]. Such asymmetric reaction

* Corresponding authors.
** Corresponding author at: Electron Microscopy Laboratory, School of Physics, Peking University, Beijing 100871, China.
E-mail addresses: fxu@seu.edu.cn (F. Xu), jlqi@hit.edu.cn (J. Qi), p-gao@pku.edu.cn (P. Gao).
[1] These authors contributed equally to this work.

https://doi.org/10.1016/j.nanoen.2018.03.076
Received 17 January 2018; Received in revised form 28 March 2018; Accepted 30 March 2018
Available online 03 April 2018

pathways likely account for the low energy efficiency of general 2D metal dichalcogenide electrode materials [20,21].

Compared to the *in situ* XRD method [17], the recent advancements in *in situ* transmission electron microscopy (TEM) techniques have made possible to track the structural evolutions during the electrochemical process in electrode materials, with significantly higher spatial resolution. This has helped understand the localized phase distribution and defect-mediated solid-state phase transformations in electrode materials at an atomic level [22–26]. For example, the electrochemical intercalation process of lithium ions into MoS_2 was found to initiate with a phase transition from 2H to 1 T $LiMoS_2$, followed by a conversion reaction [27]. Subsequently, interconnected Mo nanoparticles were formed, likely changing the optical transmittance and electrical conductivity relative to pristine MoS_2 [28]. Moreover, at the early stage of sodiation in MoS_2 nanosheets, several stable/metastable phases ($Na_{.375}MoS_2$, $Na_{.625}MoS_2$, $Na_{.75}MoS_2$, $Na_{1.0}MoS_2$, and $Na_{1.75}MoS_2$) formed before the collapse of the layered structure [19], and the transformation from 2 H to 1T MoS_2 occurred when the Na content reached 0.5 [29]. Further, Na ion diffusion within the interlayers can break the continuous layered structure into a few nanometer-sized domains via the formation of high-density defects to relax the strain induced by Na ions intercalation [18]. Nevertheless, thus far, the microstructure and the dynamics of the reaction interface between the lithiated Li_xMoS_2 and pristine MoS_2, which are critical to clarify the solid-state phase transformation mechanisms, have been rarely explored and thus motivate this study.

In this work, we combine the *in situ* TEM and aberration-corrected scanning TEM (STEM) to reveal the atomic structure and dynamic behaviors of the reaction interface during lithium ions migration in MoS_2 nanostructures. Reversible lithium ions insertion into and extraction from MoS_2 is observed. The lithium ion intercalation in MoS_2 is found to induce complicated phase transformations, forming co-existing phases of a pristine 2 H, a shrank (−3.3% (±2.3%)) 1 T phase, and an expanded (5.5% ± (2.5%)) 1T′ that is accompanied with ordered Mo clusters. The diffusivity of lithium ions in MoS_2 is measured to be in the range of ~1000–30,000 nm^2/s, which is significantly greater than that of sodium ions insertion, indicating that MoS_2 would have better electrochemical performance for lithium ion batteries compared to that for sodium ion batteries. Faster diffusion on the surface but slower diffusion in the interior leading to a "core-shell" configuration at the reaction front is also observed. The findings of this study reveal the microstructure and dynamic behaviors of the reaction interface during lithium ions migration in MoS_2 and shed light on the mechanistic understanding of solid-state phase transformations in general alkali-metal-ion batteries with transition metal dichalcogenide as electrode materials.

2. Experimental setup

2.1. In situ TEM experiments

The *in situ* TEM experimental setup comprises a layered MoS_2 as the working electrode, a lithium metal as the counter electrode, and a thin layer Li_xO (~700–1000 nm) [30] as the solid electrolyte. A half Cu grid acting as a current collector is employed to scratch the surface of the lamellar MoS_2, which is mechanically peeled off from a single crystal. The metal lithium is scratched by using an electrochemically etched, sharp tungsten tip. Both the tungsten tip and the half Cu grid are placed in an electrical TEM specimen holder (PicoFemto) in an argon-filled glovebox and then transferred into the TEM column. During the transfer process, the lithium probe was intentionally exposed to the air to form Li_xO on the surface. The exposure time is ~5 s to control the thickness of Li_xO layer [30]. Since Li_2O is a good Li^+ conductor (with the diffusivity of Li^+ in Li_2O being 10^{-10} cm^2 s^{-1} [30]) and electronic insulator (with a large band gap of ~8 eV [31]), the formed Li_xO can act as a solid-state electrolyte. The grounded tungsten tip is driven by a piezo-ceramic manipulator to contact with the MoS_2 on the edge of the half Cu grid. The lithiation of MoS_2 is achieved by applying a small

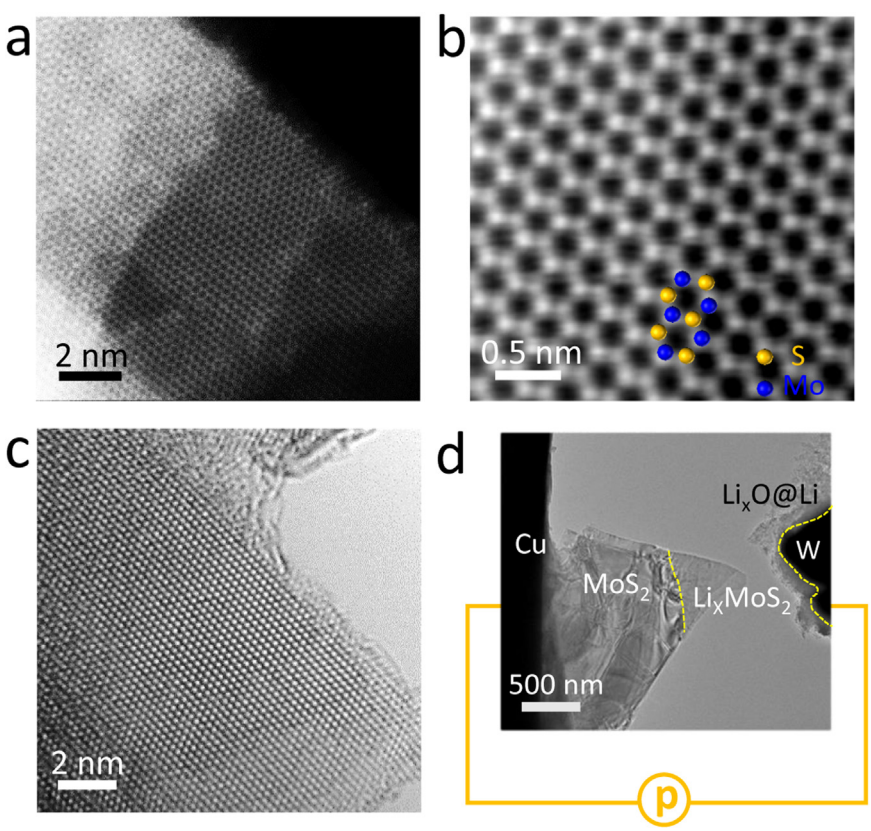

Fig. 1. Probing the structure and dynamics of the reaction interface during lithium ion migration in MoS_2 nanosheet by combining *in situ* TEM and aberration-corrected scanning TEM (STEM) method. (a) Z-contrast STEM image of MoS_2 seen along the [001] zone axis, (b) Enlarged view of the STEM image in (a), showing the arrangement of Mo (blue) and S (orange) atoms locating at different hexagonal positions, (c) High-resolution TEM (HRTEM) image of MoS_2 nanosheet, and (d) *in situ* TEM experimental setup.

negative bias (−2 V) between the grounded tungsten probe and the Cu grid, while a small positive bias (3 V) is employed to delithiate.

In situ high-resolution transmission electron microscopy (HRTEM) analysis, dark field (DF) analysis, and selected area electron diffraction (SAED) were carried out using Tecnai F20 at 200 kV equipped with an OneView IS (Gatan) camera with frame rates up to 300 frames per second. The atomically resolved STEM images are acquired using an aberration-corrected FEI Titan Themis G2 microscope operated at an accelerating voltage of 80 kV with a beam current of 80 pA, a convergence semi-angle of 25 mrad, and a collection semi-angle snap in the range of is 53–260 mrad.

2.2. Electrochemical measurements

MoS_2 was purchased from Alfa Aesar Company. The electrode was prepared by mixing MoS_2 (80 wt%), carbon black (10 wt%), and polyvinylidene fluoride (PVDF, 10 wt%) in a solution of N-methylpyrrolidone (NMP) to form a homogenous slurry. The slurry was then cast onto a clear copper foil before drying in vacuum at 80 °C for 12 h. The weight of the electrode materials was approximately 2.0 mg/cm^2. An electrolyte (1 M $LiPF_6$; ethylene carbonate (EC): dimethyl carbonate (DMC) = 50:50 vol%) was used for the lithium ion batteries. For the sodium ion batteries, sodium metal and glass fiber were used as the anode and the separator, respectively. In this case, 1 M $NaPF_6$ in a mixture of EC and DMC (EC: DMC = 50:50 vol%) was used as the electrolyte. 2032 coin cells were assembled in an argon-filled glovebox (O_2 < 0.5 ppm; H_2O < 0.5 ppm). The batteries were galvanostatically discharged and charged at a current density of 100 mA/g on a LAND CT2001A cell test apparatus at room temperature. Cyclic voltammograms (CV) analyses were carried out in the ranges of 0.7–3 V (vs Li^+/Li) and 0.2–3 V (vs Na^+/Na) with a scanning speed in the range of 0.1–0.5 mV/s.

2.3. Data acquisition and analysis

The TEM images and electron diffraction (ED) patterns were acquired using the OneView IS (Gatan) camera. The movies were prepared from continuous images acquired with different frames per second. The simulations of the ED pattern and atomistic models were performed using Crystalmaker software. The fast Fourier transform (FFT) and inversed FFT patterns were obtained using DigitalMicrograph (Gatan) software. The lithium ions intercalation domain in the DF image is measured using ImageJ. The plots were prepared by using Origin 8.0, and the error bar is determined by the full width of half-maximum of intensity peak in the profiles lines.

3. Results and discussion

Fig. 1 shows the schematic of the setup employed for *in situ* TEM experiments. The nanosheets exhibit good crystallinity along the [001] viewing direction, as observed from the STEM and HRTEM images (Fig. 1**(a)–(c)**). The atomically resolved Z-contrast image shows that the pristine MoS_2 has a hexagonal structure with sulphur and

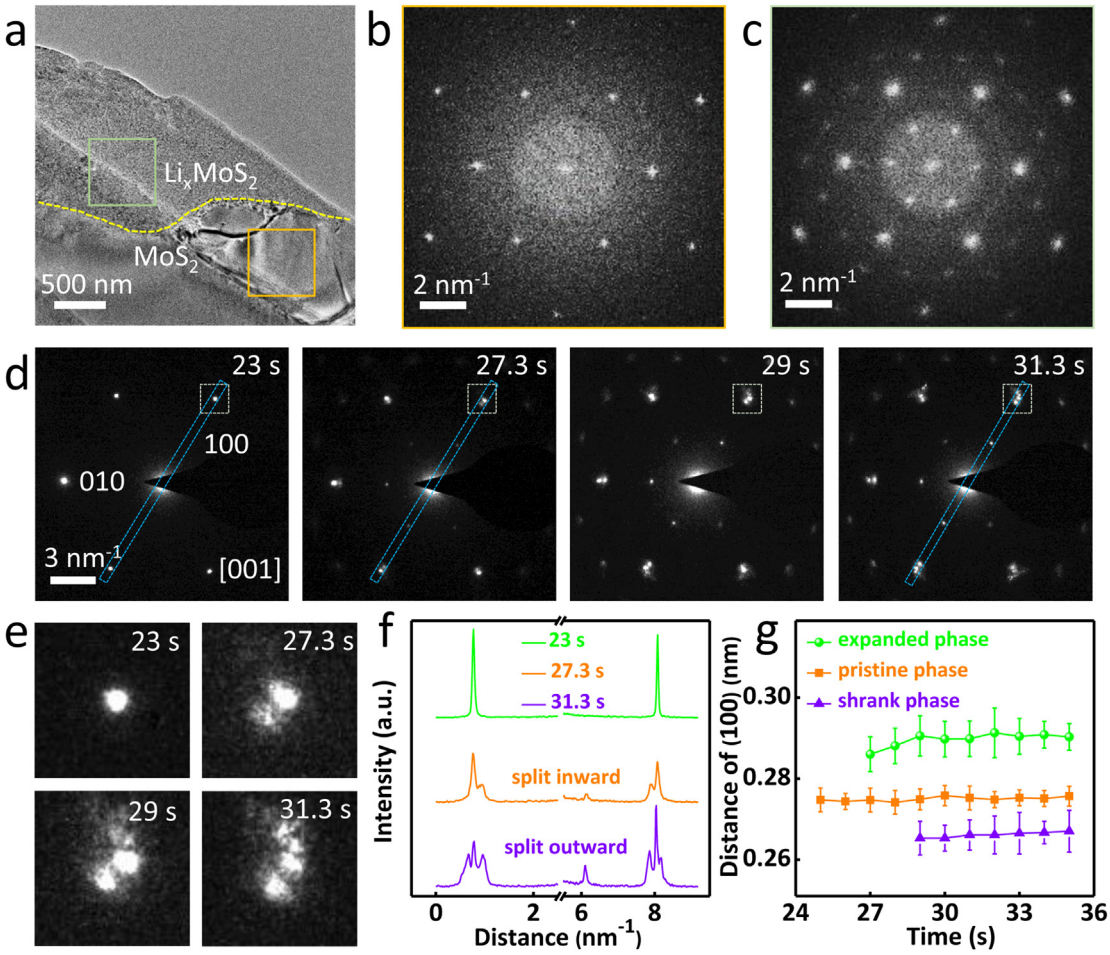

Fig. 2. Electron diffraction for tracking the structural evolution during lithium ions migration in MoS_2 nanosheet. (a) TEM image of the interface after the lithium ions insertion, FFT images of the regions from (b) pristine MoS_2, and (c) Li_xMoS_2 as marked by the squares in (a); (d) Time-lapsed electron diffraction images of *in situ* lithiated MoS_2 along the [001] zone axis, and (e) Corresponding evolution process of (100) diffraction spot, and (f) Intensity profiles taken along the blue dashed rectangles in (d). (g) Lithium-ions-insertion-induced lattice changes measured from (100)-MoS_2 diffraction spot.

molybdenum atoms locating at different hexagonal positions (Fig. 1**(b)**). Fig. 1**(d)** shows a typical TEM image of a nanosized solid battery cell consisting of MoS_2 nanosheets (as the working electrode), a Li counter electrode, and a solid-state electrolyte (in the form of a passivation Li_xO layer).

Upon lithium ions insertion, a clear phase boundary between Li_xMoS_2 and MoS_2 can be observed, as shown in Fig. 2**(a)**. The FFT pattern of the reacted Li_xMoS_2 (Fig. 2**(c)**) shows additional superstructure spots, compared to that of the pristine MoS_2 (Fig. 2**(b)**), suggesting the formation of new phases. To quantify the structural evolutions at the reaction interface, time-series *in situ* electron diffraction patterns was recorded during lithium ions intercalation (Fig. 2**(d)–(f)** and Movie S1). Unlike the HRTEM imaging, electron diffraction can be applied to a much larger area to minimize the effects of the electron beam, particularly given that MoS_2 nanosheets are sensitive to electron beam illumination [19]. The SAED pattern of pristine 2H-MoS_2, shown in Fig. S1b, is identified to be oriented along the [001] zone axis, consistent with the simulated electron diffraction pattern, shown in Fig. S1c.

Supplementary material related to this article can be found online at http://dx.doi.org/10.1016/j.nanoen.2018.03.076.

Upon lithium ions intercalation, the diffraction spot (100) firstly splits inward, and subsequently outward. Finally, they appear as three weak, separated diffraction spots, as shown in Fig. 2**(e)** and 2**(f)**, indicating the formation of new phases. Moreover, Fig. S2 shows the (010) diffraction spot also firstly splits inward and then outward. Note that the inward split of the diffraction spots implies an increased lattice constant and an outward split indicates a decreased lattice constant. Fig. 2**(g)** shows the evolution of the lattice distance as a function of the time, wherein the three phases co-exist at the interface upon lithium ions intercalation, i.e., pristine 2 H phase, shrank 1T phase, and expanded 1T′ phase. The average variations for the shrank 1T phase and expanded 1T′ phase are − 3.3% (± 2.3%) and 5.5% (± 2.5%), respectively, as shown in Fig. S3. Furthermore, the equivalent diffraction spots from the same family of crystal planes split differently in terms of the split time. Particularly, in Fig. S4, the (100) diffraction spot splits inward at 27 s, whereas the (010) diffraction spot splits inward after 1.6 s. Moreover, the (100) diffraction spot splits into three ones at 31 s, whereas the (010) diffraction spot splits into three ones after 1.6 s. Note that spot splitting first indicates lithium ions diffuse along the corresponding direction preferentially. Due to the irregular shape of the contact point, the applied small bias causing inhomogeneous electrical fields along different directions is likely related with the preferential lithiation diffusion, although further studies are needed to fully understand such behavior. Such heterogeneous spots split is observed in most cases in the experiments as shown in Fig. S5. Note that such details of the equivalent diffraction spots from the same family of crystal planes cannot be revealed from an *in situ* XRD experiment that can only provide averaged information over a large region.

The structure of the reaction interface is further analyzed using HRTEM and STEM images, as shown in Fig. 3. A clear boundary between the pristine MoS_2 and lithiated Li_xMoS_2 is observed, as shown in Fig. S6a. The FFT pattern of the pristine MoS_2 phase (Fig. S6b) is identified to be along the [03-1] zone axis, whereas the FFT pattern of the Li_xMoS_2 phase (Fig. S6c) exhibits a 2 × 1 1 T′ structure. Atomically resolved Z-contrast image in Fig. 3**(c)** reveals the presence of alternating zigzag chains, with measured Mo-Mo distance of 0.21 nm and 0.19 nm (Fig. S7b), corresponding to 2 × 1 1 T′ structure [5,27,32]. Such Mo clusters can also lead to a 2 × 2 1 T′ structure as shown in Figs. S7**(c)–(d)**. To better understand different structures of 2 H, 1 T, 2 × 1 1 T′ and 2 × 2 1 T′ phases, ball and stick models [27] are shown in Fig. 3**(d)–(g)**. Moreover, edge dislocations are also observed at the interface region, judging from the Fast Fourier space filtered image (Fig. 3**b**) [33,34]. The dislocations originate from the structural fracture of the layered structure (Fig. S8) during lithium ion migration [18].

As the lithium ion intercalation in MoS_2 leads to additional diffraction spots compared to the pristine 2 H phase, the DF TEM imaging is used to track the motion of the Li_xMoS_2/MoS_2 phase boundary. The

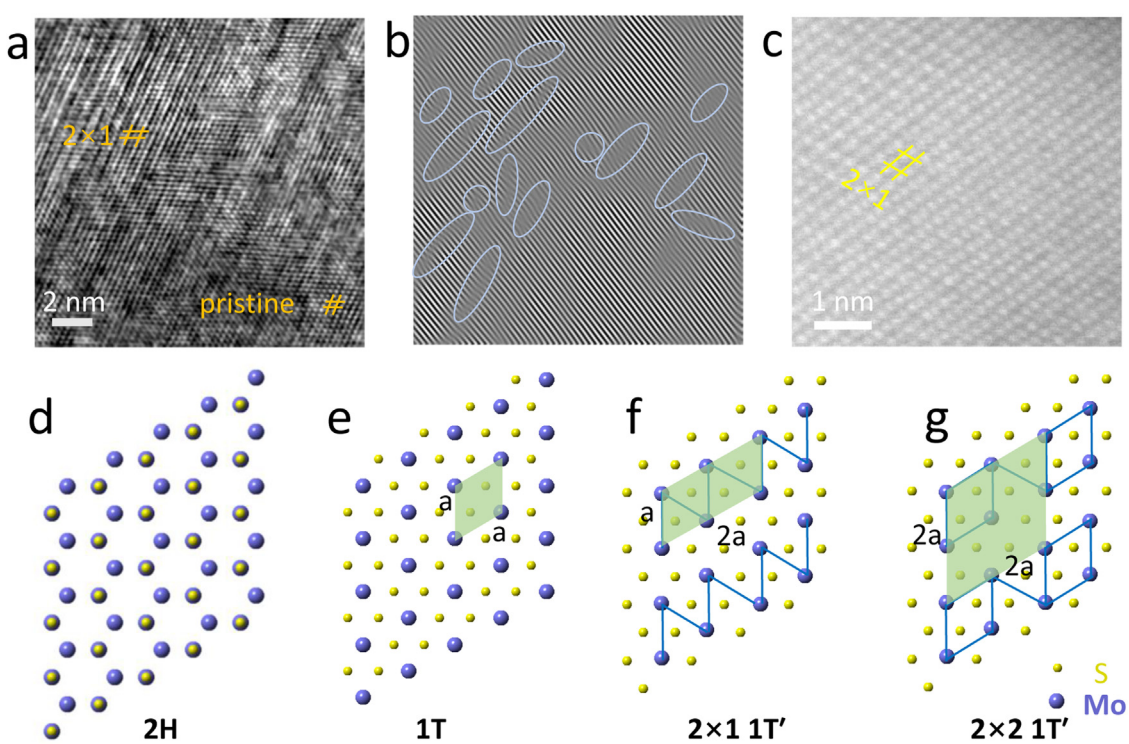

Fig. 3. Probing the structure of the reaction interface and distorted 1 T phase (called 1 T′) upon lithium ions insertion into MoS_2 nanosheet. (a) HRTEM image of the interface between 2 × 1 1 T′ Li_xMoS_2 and MoS_2, (b) Fast Fourier space filtered image using the (013) frequencies; Dislocations and defects are marked with blue outlines; (c) Z-contrast STEM image of 2 × 1 1T′ Li_xMoS_2. Schematic of the atom structure in ab plane of (d) 2H, (e) 1T, (f) 2 × 1 structure and (g) 2 × 2 structure. Distorted 2 × 1 and 2 × 2 structures are caused by different Mo clusters.

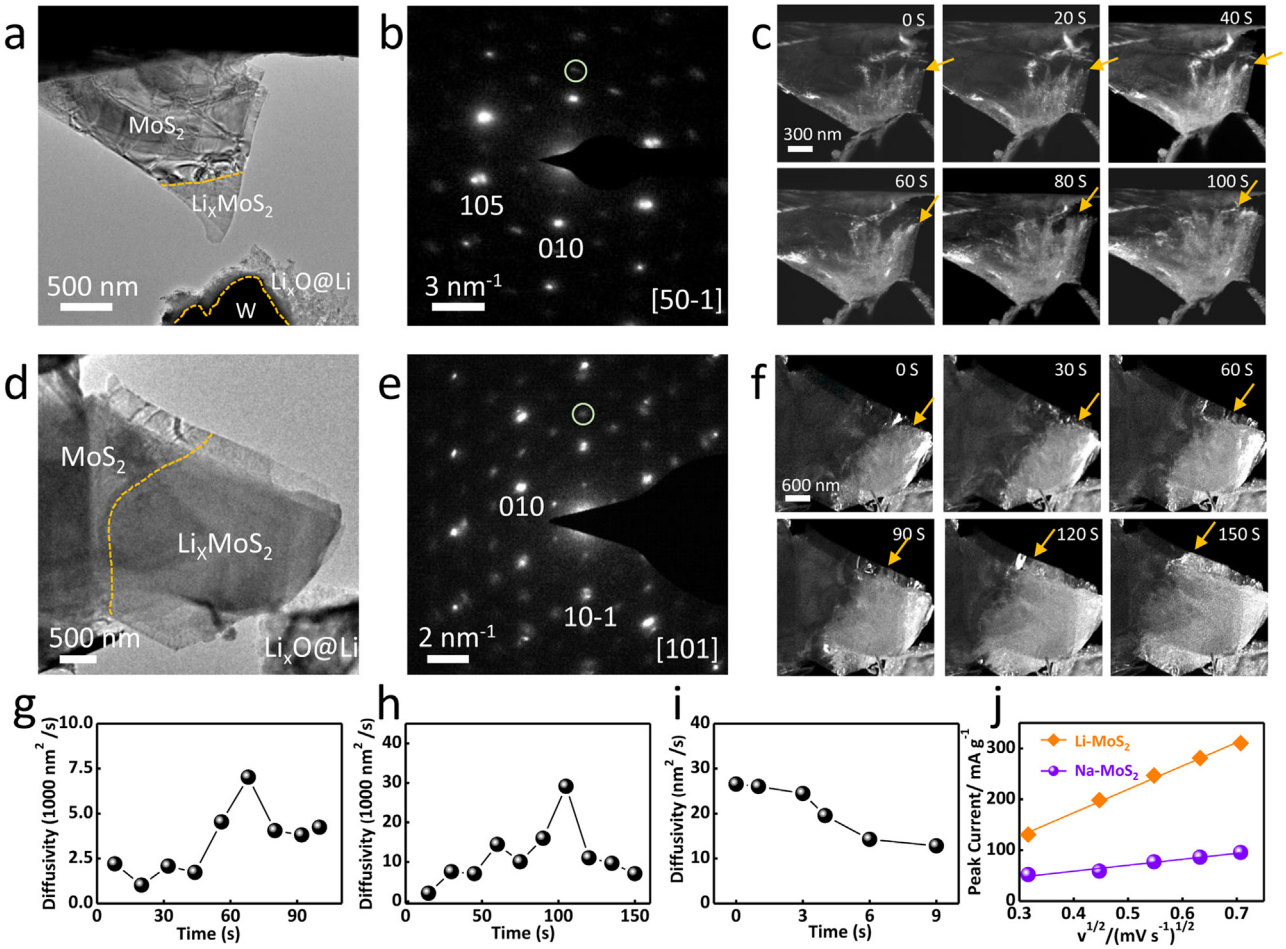

Fig. 4. Dark field (DF) imaging for tracking the reaction interface motion during lithium ion migration in MoS_2 nanosheet. (a, d) BF images showing the interface. (b, e) ED patterns of 1T′ Li_xMoS_2. The white circle highlights a superstructure reflection, which is used for dark-field imaging. (c, f) Time-series dark field images directly show the movement of the interface. The diffusivity of lithium ions (g) calculated from (c), and (h) calculated from (f), and the diffusivity of sodium ions (i) in MoS_2 [18]. (j) Peak current against square root of scan rate based on cyclic voltammograms of Li-MoS_2 and Na-MoS_2 batteries.

superstructure reflection is chosen to form the DF image. Thus, the lithium-ions-intercalated phase appears brighter, whereas the pristine 2 H phase appears to be darker, as shown in Fig. 4**(a)–(f)**, and Movies S2 and S3, which shows the lithiated process of two MoS_2 nanosheets respectively. Accordingly, in Fig. 4**(g)** and **(h)**, the diffusivity is directly measured to be ~1000–30,000 nm^2/s from the DF images and movies, based on the equation $D = d^2/2t$ [35], where D is the diffusivity, t is the diffusion time, and d is the diffusion distance. The diffusion distance is valued as the square root of the domain area associated with the lithium ion intercalation (brighter areas in the DF images). Note that the estimated diffusivity should be primitive as it also depends on the localized contact conditions which can be very different from one to another. Therefore, more precise estimations can be obtained from the electrochemical measurements of coin cell batteries as discussed below. However, it is still reasonable to conclude that the diffusivity of the lithium ions in MoS_2 is higher than that of sodium insertion (10–20 nm^2/s) as shown in Fig. 4**(i)**, which was obtained from previous work [18]. The faster lithium ion diffusion in MoS_2 is due to the lower diffusion barrier, which has been revealed by the theoritical calculations that the barrier between adjacent octahedral sites in MoS_2 for lithium ions diffusion is ~0.49 eV [36] whereas it increases to ~0.7 eV for sodium ions diffusion [37].

Supplementary material related to this article can be found online at http://dx.doi.org/10.1016/j.nanoen.2018.03.076.

The kinetics of the intercalation process plays a crucial role in determining electrochemical performances for lithium ion and sodium ion batteries. In order to more quantitatively compare the electrochemical performance (e.g. the rate and cycling performance and the diffusivity) between Li-MoS_2 and Na-MoS_2 batteries, coin cell batteries are fabricated and the electrochemical measurements are carried out. Firstly, Fig. S9a shows the galvanostatic discharge–charge curves, wherein more lithium ions intercalate into MoS_2 with a capacity of 925.3 mAh/g *vs.* 601.2 mAh/g for Na-ion intercalation (corresponding to $Li_{5.5}MoS_2$ and $Na_{3.6}MoS_2$) (Fig. S9b) when discharging, suggesting the facile kinetics process for lithium ion in MoS_2. The Li-MoS_2 battery shows a higher capacity retention of 30.78% (from 288.5 mAh g^{-1} to 88.8 mAh g^{-1}) after 73 cycles, while the capacity retention for the Na-MoS_2 battery is 21.3% (from 203.5 mAh g^{-1} to 43 mAh g^{-1}) in Fig. S9c. Moreover, the rate performance in Fig. S9d indicates the discharge capacity for Li-MoS_2 at different rates is better than that of Na-MoS_2.

Secondly, the ion diffusion in the solid state obeys the Randles–Sevcik relationship [38,39],

$$I_p = 0.4463 n^{3/2} F^{3/2} C_{Li} S R^{-1/2} T^{-1/2} D_{Li}^{1/2} v^{1/2} \quad (1)$$

wherein I_p is the peak current (A), n is the amount of electron exchange for the considered redox couple, F is the Faraday constant (96485.4 C mol^{-1}), C_{Li} is the Li-ion concentration, S is the surface area of the electrode (0.785 cm^2), R is the gas constant (8.314 J mol^{-1} K^{-1}), T is the absolute temperature (273.15 K), D_{Li} is the chemical diffusion coefficient (cm^2 s^{-1}), and v is the scanning rate (V s^{-1}). The theoretical molar volume of MoS_2 is 32 cm^3, equaling to 0.03125 mol cm^{-3} [40]. From the cyclic voltammograms between 0.7–3.0 V for Li-MoS_2 and

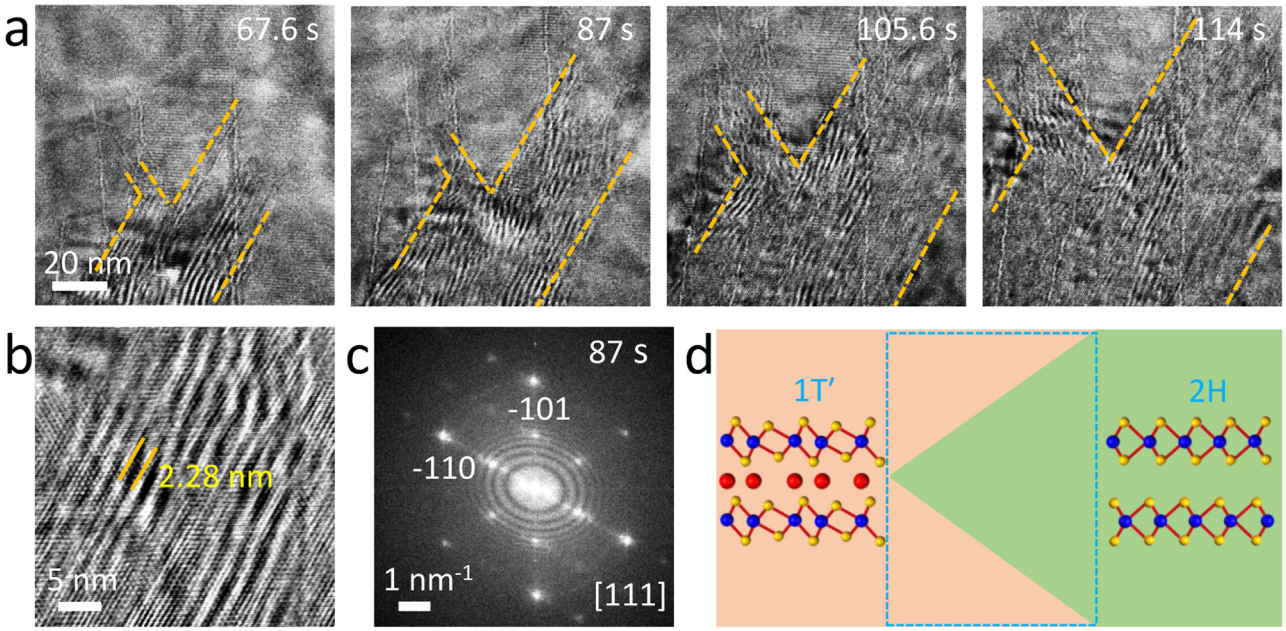

Fig. 5. High-resolution imaging for tracking the reaction interface motion during lithium ion migration in a relatively thick MoS_2 nanosheet. (a) Evolution of stripes at the reaction interface upon lithium insertion, (b) HRTEM image of the Moiré stripes, (c) FFT image of (a) taken at 87 s, and (d) Schematic of the core-shell-like structure, explaining the formation of the secondary electron diffraction at the reaction front.

0.2–3.0 V for Na-MoS_2 batteries as shown in Figs. S9e and S9f, the slope of the peak current against square root of scan rate can be acquired (Fig. 4**j**). Based on the Eq. (1), the diffusion coefficients for Li^+ and Na^+ in MoS_2 are calculated as 5.4×10^{-12} cm^2 s^{-1} (540 nm^2 s^{-1}) and 3.5×10^{-13} cm^2 s^{-1} (35 nm^2 s^{-1}), which is the same level from the previous report (2.02×10^{-13} cm^2 $s^{-1}$for Na^+ diffusion in MoS_2) [41]. It should be noted that the estimated values from *in situ* TEM experiments only reflect the migration process in the interior of electrode, while the process to across the solid-electrolyte interface is ignored. This fact may partly account for the difference between microscopic (*in situ* TEM) and macroscopic (electrochemical test for coin cells) measurements.

The HRTEM image series are obtained to reveal the local structural evolutions upon lithium ions insertion, as shown in Fig. 5**(a)** and Movie S4, wherein lattice stripes with an average spacing of 2.28 nm (Fig. 5**(b)**) are observed at the reaction front with the viewing direction from [111] zone axis, judging from FFT pattern in Fig. 5**(c)**. These Moiré stripes are mainly derived from the lattice mismatch between MoS_2 and lithiated MoS_2 [42,43], which are related to the secondary electron diffraction which occurs when the electron beam passes through two crystal materials with different lattice constants [44,45]. Generally, the lithium ions diffusion on the surface occurs easily and is faster than that inside, because of the lower barrier at the surface [46], forming a core-shell-like structure at the reaction front. In fact, similar

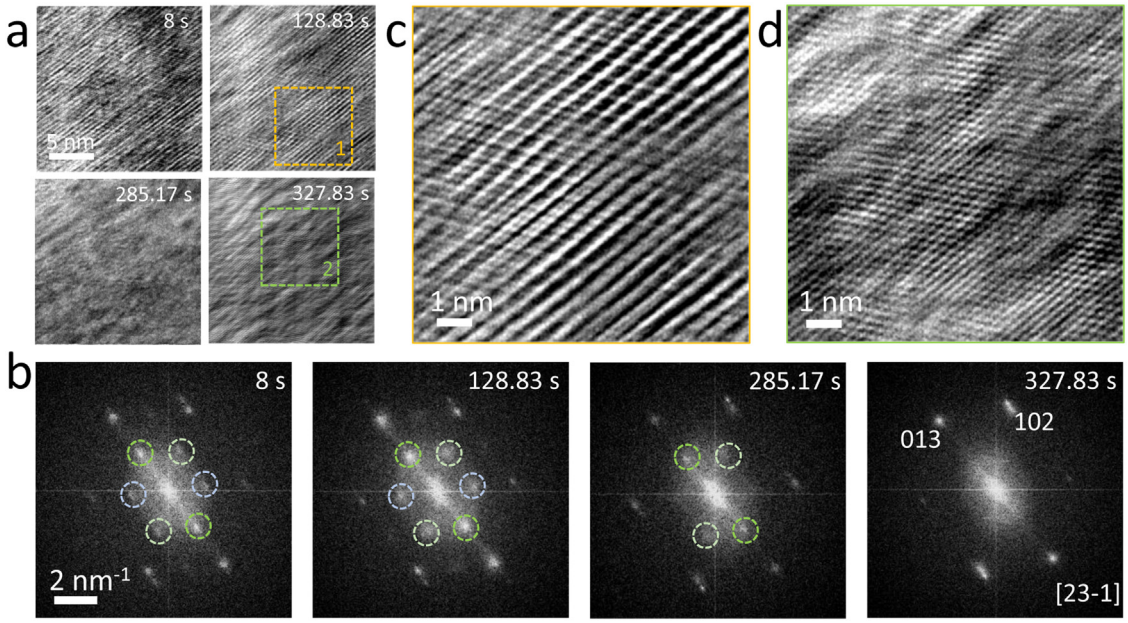

Fig. 6. High resolution imaging tracking process of delithiation for Li_xMoS_2. (a) Selected HRTEM image series showing the structure evolutions during delithiation. (b) The corresponding FFT patterns. (c) HRTEM image of region1 in (a), showing a 2 × 2 structure. (d) HRTEM image of region 2 in (a), showing a pristine MoS_2 structure.

phenomena were observed in SnO_2 nanowire during lithiation [47,48]. Previous first principles calculations have shown that the surface sites of Si nanowires are energetically the most favorable locations for lithium ions insertion [49]. In our experiments, the core is the pristine 2 H MoS_2 phase, surrounded by 1T′ Li_xMoS_2, as shown in the projected schematic in Fig. 5**(d)**. The electron beam first passes through the top 1T′ Li_xMoS_2 layer, followed by the middle pristine 2H MoS_2 layer, and finally reaches the bottom 1T′ Li_xMoS_2 layer. The diffracted beam exited from the top 1T′ Li_xMoS_2 layer serves as the transmission beam for the middle 2H phase, leading to secondary electron diffraction. Note that the lattice mismatch (~5.5%) between MoS_2 and lithiated MoS_2, as shown in Fig. S10, satellite spots appear in the FFT patterns [50,51]. Consequently, the Fast Fourier space filtered image (Fig. S11b) appears to be similar to that of the TEM image (Fig. S11a). Moreover, it is noteworthy that the propagation of the stripes is not uniform, as shown in Fig. 5**(a)**. The lithium ions tend to propagate along the [−1–12] direction firstly and subsequently along the [−211] direction, probably because of the non-uniform electrochemical potential gradients.

Supplementary material related to this article can be found online at http://dx.doi.org/10.1016/j.nanoen.2018.03.076.

The complete extraction of the lithium ions (charging) is a prerequisite for rechargeable lithium ion batteries. We found that once the insertion of Li ions into MoS_2 is controlled within the intercalation range, as shown in Fig. S12, the lithium ions in Li_xMoS_2 can be partly extracted, as shown in Fig. 6 and Movies S5 and S6. From series of HRTEM images and corresponding FFT images(Fig. 6**(a)** and **(b)**) viewing along the [23−1] zone axis, we can find the superstructure spots gradually vanish, suggesting the extraction of lithium ions. Moreover, as shown in Fig. 6**(c)** and **(d)**, after applying a positive bias for 327 s, the lithiated 2 × 2 modulated Li_xMoS_2 structure vanishes. Further, *in situ* DF movies (Movie S7) also shows only partial lithium ions can be slowly extracted. Unlike the fast lithiation process, the delithiation process is significantly slower, because lithium ion extraction corresponds to charge and thus is unfavorable. Accordingly, the coulombic efficiency for Li-MoS_2 batteries is low, i.e., 53.52% and 49.81% for the first two cycles calculated from the galvanostatic discharge–charge curves, as shown in Fig. S9b. Note that previous studies also reported that the fully reversible delitiation is usually difficult due to the specific experimental setup with point contact [52]. One possible reason is that from this setup the external potential mainly concentrates near the probe thus cannot pull those distant ions back to the anode during charging. Further improvements are needed to achieve fully reversible phase transitions.

Supplementary material related to this article can be found online at http://dx.doi.org/10.1016/j.nanoen.2018.03.076.

The above results demonstrate that lithium ion insertion in MoS_2 leads to a series of phase transformations forming distinct co-existing phases including a shrank (~–3.3% (± 2.3%)) 1T phase and an expanded (~5.5% (± 2.5%)) 1T′ phase. The presence of these phases is confirmed from both ED patterns and HRTEM images. The small changes in the lattice constants remove significant volume change and thus enable good structural stability during cycling in practical batteries. The structural phase transformation from 2H to 1T phase is accompanied with an electronic phase change. Once the 1 T phase is formed, the enhanced conductivity of the 1 T phase likely facilitates the ionic migration. The lithium ions diffusion in MoS_2 is measured to be in the range of ~1000–30,000 nm^2/s. A faster diffusion on the surface of MoS_2 leads to the formation of a structure with a MoS_2 core and a Li_xMoS_2 shell at the reaction interface. Such a fast ionic diffusion enables to achieve high power and facilitate fast cycling of batteries with MoS_2, if the electrode materials are appropriately engineered.

4. Conclusions

The atomic structure and dynamics of the reaction interface between the lithiated Li_xMoS_2 and pristine MoS_2 are systematically studied by combining the *in situ* TEM techniques and aberration-corrected TEM. Upon lithium ions intercalation, two-phase transformations occur at the interface, wherein three co-existing phases are identified, i.e. the pristine 2 H phase, shrank (~–3.3% ± (2.3%)) 1 T phase, and expanded (~5.5% ± (2.5%)) 1T′ phase. The atomic structure of the 1T′ phase with superstructure reflections in the diffraction pattern is caused by the Mo distortion. The diffusivity of the lithium ion in MoS_2 is ~1000–30,000 nm^2/s, which is greater than that of sodium diffusion (10–20 nm^2/s). The lithium ions diffusion is faster on the surface of MoS_2, forming a structure with a MoS_2 core and a Li_xMoS_2 shell at the reaction interface. Dislocations are also observed at the interface because of the structural fracture induced by lithium ions migration. Moreover, once lithium ions insertion is controlled within intercalation, lithium ion extraction can be partly achieved. This study reveals the structure and dynamics of the MoS_2/Li_xMoS_2 reaction interface. These findings would help understand the structure and properties of transition-metal dichalcogenides as electrode materials for battery applications.

Acknowledgments

The work was supported by the National Natural Science Foundation of China [Grant numbers 51575135, U1537206, 11771051, 61574034, 51502007, and 51672007]; National Basic Research Program of China [Grant numbers 2016YFA0300804 and 2016YFA0300903]; National Equipment Program of China [Grant number ZDYZ2015-1] and “2011 Program” Peking-Tsinghua-IOP Collaborative Innovation Center of Quantum Matter. We gratefully acknowledge Gatan for providing the OneView IS (Gatan, Inc.) camera as well as for the technique help and Electron Microscopy Laboratory in Peking University for the use of Cs corrected electron microscope.

Appendix A. Supplementary material

Supplementary data associated with this article can be found in the online version at http://dx.doi.org/10.1016/j.nanoen.2018.03.076.

References

[1] J. Xiao, D. Choi, L. Cosimbescu, P. Koech, J. Liu, J.P. Lemmon, Chem. Mater. 22 (2010) 4522–4524.
[2] J. Xiao, X. Wang, X. Yang, S. Xun, G. Liu, P.K. Koech, J. Liu, J.P. Lemmon, Adv. Funct. Mater. 21 (2011) 2840–2846.
[3] K. Chang, W. Chen, ACS Nano 5 (2011) 4720–4728.
[4] X. Xie, Z. Ao, D. Su, J. Zhang, G. Wang, Adv. Funct. Mater. 25 (2015) 1393–1403.
[5] M. Chhowalla, H.S. Shin, G. Eda, L. Li, K.P. Loh, H. Zhang, Nat. Chem. 5 (2013) 263–275.
[6] E. Benavente, M.A. Santa Ana, F. Mendizábal, G. González, Coord. Chem. Rev. 224 (2002) 87–109.
[7] Y. Li, Y. Liang, F.C. Robles Hernandez, H. Deog Yoo, Q. An, Y. Yao, Nano Energy 15 (2015) 453–461.
[8] Z. Zhang, W. Li, M.F. Yuen, T. Ng, Y. Tang, C. Lee, X. Chen, W. Zhang, Nano Energy 18 (2015) 196–204.
[9] Z. Shi, W. Kang, J. Xu, Y. Sun, M. Jiang, T. Ng, H. Xue, D.Y.W. Yu, W. Zhang, C. Lee, Nano Energy 22 (2016) 27–37.
[10] B. Chen, Y. Meng, F. He, E. Liu, C. Shi, C. He, L. Ma, Q. Li, J. Li, N. Zhao, Nano Energy 41 (2017) 154–163.
[11] F. Wypych, C. Solenthaler, R. Prins, T. Weber, J. Solid State Chem. 144 (1999) 430–436.
[12] F. Wypych, R. Schollhorn, J. Chem. Soc., Chem. Commun. 19 (1992) 1386–1388.
[13] M.A. Py, R.R. Haering, Can. J. Phys. 61 (1983) 76–84.
[14] Y. Lin, D.O. Dumcenco, Y. Huang, K. Suenaga, Nat. Nanotechnol. 9 (2014) 391–396.
[15] R. Bissessur, M.G. Kanatzidis, J.L. Schindler, C.R. Kannewurf, J. Chem. Soc., Chem. Commun. 20 (1993) 1582–1585.
[16] L.F. Mattheiss, Phys. Rev. B 8 (1973) 3719–3740.
[17] X. Wang, X. Shen, Z. Wang, R. Yu, L. Chen, ACS Nano 8 (2014) 11394–11400.
[18] P. Gao, L. Wang, Y. Zhang, Y. Huang, K. Liu, ACS Nano 9 (2015) 11296–11301.
[19] Q. Li, Z. Yao, J. Wu, S. Mitra, S. Hao, T.S. Sahu, Y. Li, C. Wolverton, V.P. Dravid, Nano Energy 38 (2017) 342–349.
[20] P. Gao, Y. Zhang, L. Wang, S. Chen, Y. Huang, X. Ma, K. Liu, D. Yu, Nano Energy 32 (2017) 302–309.
[21] P. Gao, L. Wang, Y. Zhang, Y. Huang, L. Liao, P. Sutter, K. Liu, D. Yu, E. Wang, Nano Lett. 16 (2016) 5582–5588.
[22] J. Li, K. He, Q. Meng, X. Li, Y. Zhu, S. Hwang, K. Sun, H. Gan, Y. Zhu, Y. Mo,

E.A. Stach, D. Su, ACS Nano 10 (2016) 9577–9585.
[23] F. Xu, Z. Li, L. Wu, Q. Meng, H.L. Xin, J. Sun, B. Ge, L. Sun, Y. Zhu, Nano Energy 30 (2016) 771–779.
[24] M.T. McDowell, Z. Lu, K.J. Koski, J.H. Yu, G. Zheng, Y. Cui, Nano Lett. 15 (2015) 1264–1271.
[25] X.H. Liu, H. Zheng, L. Zhong, S. Huang, K. Karki, L.Q. Zhang, Y. Liu, A. Kushima, W.T. Liang, J.W. Wang, J. Cho, E. Epstein, S.A. Dayeh, S.T. Picraux, T. Zhu, J. Li, J.P. Sullivan, J. Cumings, C. Wang, S.X. Mao, Z.Z. Ye, S. Zhang, J.Y. Huang, Nano Lett. 11 (2011) 3312–3318.
[26] K. He, S. Zhang, J. Li, X. Yu, Q. Meng, Y. Zhu, E. Hu, K. Sun, H. Yun, X. Yang, Y. Zhu, H. Gan, Y. Mo, E.A. Stach, C.B. Murray, D. Su, Nat. Commun. 7 (2016) 11441–11449.
[27] L. Wang, Z. Xu, W. Wang, X. Bai, J. Am. Chem. Soc. 136 (2014) 6693–6697.
[28] J. Wan, W. Bao, Y. Liu, J. Dai, F. Shen, L. Zhou, X. Cai, D. Urban, Y. Li, K. Jungjohann, M.S. Fuhrer, L. Hu, Adv. Energy Mater. 5 (2015) 1401742.
[29] Q. Huang, X. Li, M. Sun, L. Zhang, C. Song, L. Zhu, P. Chen, Z. Xu, W. Wang, X. Bai, Adv. Mater. Inter. (2017) 1700171.
[30] X.H. Liu, J.Y. Huang, Energy Environ. Sci. 4 (2011) 3844.
[31] M.M. Islam, T. Bredow, C. Minot, J. Phys. Chem. B 110 (2006) 9413.
[32] S.J.R. Tan, I. Abdelwahab, Z. Ding, X. Zhao, T. Yang, G.Z.J. Loke, H. Lin, I. Verzhbitskiy, S.M. Poh, H. Xu, C.T. Nai, W. Zhou, G. Eda, B. Jia, K.P. Loh, J. Am. Chem. Soc. 139 (2017) 2504.
[33] S.I. Kim, K.H. Lee, H.A. Mun, H.S. Kim, S.W. Hwang, J.W. Roh, D.J. Yang, W.H. Shin, X.S. Li, Y.H. Lee, G.J. Snyder, S.W. Kim, Science 348 (2015) 109.
[34] Y.L. Hao, S.J. Li, M.L. Sui, D.X. Li, R. Yang, J.P. Cui, Phys. Rev. Lett. 102 (2009) 45503.
[35] J.C. Thomas, Q. Xu, B. Swoboda, D. Morgan, A. Van der Ven, Phys. Rev. B 78 (2008) 104306.
[36] Y. Li, D. Wu, Z. Zhou, C.R. Cabrera, Z. Chen, J. Phy, Chem. Lett. 3 (2012) 2221–2227.
[37] J.C. Su, Y. Pei, Z.H. Yang, X.Y. Wang, RSC Adv. 4 (2014) 43183–43188.
[38] X. Dai, L. Wang, J. Xu, Y. Wang, A. Zhou, J. Li, ACS Appl. Mater. Inter. 6 (2014) 15853.
[39] L. Wang, J. Xu, C. Wang, X. Cui, J. Li, Y. Zhou, RSC Adv. 5 (2015) 71684.
[40] Y. Miki, D. Nakazato, H. Ikuta, T. Uchida, M. Wakihara, J. Power Sources 54 (1995) 508.
[41] Y. Li, Y. Liang, F.C. Robles Hernandez, H. Deog Yoo, Q. An, Y. Yao, Nano Energy 15 (2015) 453.
[42] X. Zhou, J. Shi, Y. Qi, M. Liu, D. Ma, Y. Zhang, Q. Ji, Z. Zhang, C. Li, Z. Liu, Y. Zhang, ACS Nano 10 (2016) 3461.
[43] C.W. Sun, J.S. Jeong, J.Y. Lee, J. Cryst. Growth 294 (2006) 162.
[44] M.C.A.A.J. Proc, Phys. Soc. Lond. A 64 (1951) 609.
[45] C.B. Carter, D.B. Williams, Transmission Electron Microscopy: a Textbook for Materials Science, Spring, Germany, 2009.
[46] C. Uthaisar, V. Barone, Nano Lett. 10 (2010) 2838–2842.
[47] J.Y. Huang, L. Zhong, C.M. Wang, J.P. Sullivan, W. Xu, L.Q. Zhang, S.X. Mao, N.S. Hudak, X.H. Liu, A. Subramanian, H. Fan, L. Qi, A. Kushima, J. Li, Science 330 (2010) 1515–1520.
[48] X.H. Liu, H. Zheng, L. Zhong, S. Huang, K. Karki, L.Q. Zhang, Y. Liu, A. Kushima, W.T. Liang, J.W. Wang, J. Cho, E. Epstein, S.A. Dayeh, S.T. Picraux, T. Zhu, J. Li, J.P. Sullivan, J. Cumings, C. Wang, S.X. Mao, Z.Z. Ye, S. Zhang, J.Y. Huang, Nano Lett. 11 (2011) 3312.
[49] Q. Zhang, W. Zhang, W. Wan, Y. Cui, E. Wang, Nano Lett. 10 (2010) 3243–3249.
[50] Q. Jeangros, A. Faes, J.B. Wagner, T.W. Hansen, U. Aschauer, J. Van Herle, A. Hessler-Wyser, R.E. Dunin-Borkowski, 58, 2010, pp. 4578–4589.
[51] J. Wintterlin, M.L. Bocquet, Surf. Sci. 603 (2009) 1841–1852.
[52] Y. Zhu, J.W. Wang, Y. Liu, X. Liu, A. Kushima, Y. Liu, Y. Xu, S.X. Mao, J. Li, C. Wang, J.Y. Huang, Adv. Mater. 25 (2013) 5461.

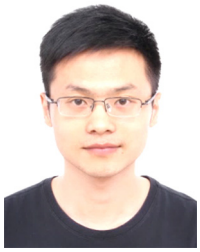

Shulin Chen is currently a Ph.D. candidate in School of Materials Science, Harbin Institute of Technology. He received his Bachelor's degree from Harbin Institute of Technology in 2015. He joined Prof. Peng Gao's group in 2016. His research interests are the defects and the interface of 2D material and the structure-property relationships of energy storage by using transmission electron microscopy.

Liping Wang is currently an associate professor in University of Electronic Science and Technology of China. She received her Ph.D. degrees (2011) in Institute of Physics, Chinese Academy of Sciences and Laboratoire de réactivité et chimie des solides, Université de Picardie Jules Verne, France. She worked as a post-doctoral fellow in Max Planck Institute of Colloids and Interfaces, Germany (2012) and a research associate at Brookhaven National Lab, United States (2013–2014). Her current research interests are structure-property correlations of electrode materials as energy storage devices.

Ruiwen Shao is a postdoctor in School of Physics, Peking University. He received his Ph.D. degree in condensed mater physics from the Institute of Microstructure and Properties of Advanced Materials, Beijing University of Technology in 2016. His research interests are the structure-property relationships of 2D material and the *in situ* TEM observation of electrochemical behaviors of nanomaterials

Jian Zou is a graduate student in School of Materials and Energy, University of Electronic Science and Technology of China. His current interests are potassium ion batteries and lithium metal surface modification.

Ran Cai received her bachelor degree in Polymer Materials Science and Engineering from Nanjing University of Posts and Telecommunications in 2013. She is now a Ph.D. candidate at Key laboratory of MEMS of Ministry of Education, Southeast University. Her research interest is the *in situ* TEM observation of electrochemical behaviors of nanomaterials.

Jinghuang Lin is a Ph.D. candidate under the supervision of Prof. Jicai Feng and Prof. Junlei Qi in Harbin Institute of Technology. His research mainly focuses on the carbon nanomaterials and transition metal compounds for energy storage devices.

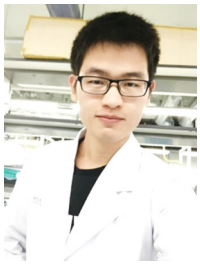

Chongyang Zhu is currently pursuing his Ph.D. degree at Key laboratory of MEMS of Ministry of Education, Southeast University, Nanjing. He received his bachelor degree in Polymer Materials Science and Engineering from Nanjing University of Posts and Telecommunications in 2013. His research interests involve the *in situ* TEM characterizations of nanomaterials under vacuum and liquid environment.

Jingmin Zhang accepted his Ph.D. in the field of material physics from Martin-Luther University in Germany in 2004. He is currently serving as an engineer for Electron Microscopy Laboratory of school of physics at Peking University in P.R China. His work has centered on characterization of various materials by transmission electron microscopy (TEM) techniques.

Feng Xu is a Professor at the Key Laboratory of MEMS of the Ministry of Education at Southeast University (SEU). He obtained his Ph.D. in 2009 from Nanjing Tech University and then was promoted to Associate Professor and Professor at Southeast University in 2012 and 2017, respectively. He was a Visiting Scholar at Brookhaven National Laboratory from 2014 to 2015. Currently, his research interests mainly focus on exploring the structure-activity relationship of nanomaterials by in-situ transmission electron microscopy method and their potential applications in photovoltaics, second batteries, fuel cells photodetection, etc.

Jian Cao is a professor in Harbin Institute of Technology. At present, his major researches are joining of new materials and dissimilar materials.

Jicai Feng is a professor in Harbin Institute of Technology. His research interests mainly focus on joining of new materials and dissimilar materials.

Junlei Qi is a professor in Harbin Institute of Technology. He received Ph.D. degree in Jilin University. At present, his major researches are carbon nanomaterials, metal matrix composites and transition metal compounds for energy storage devices.

Peng Gao is an assistant Professor in School of Physics, Peking University, Beijing, China. He received his Ph.D. degree in condensed mater physics from the Institute of Physics, Chinese Academy of Sciences in 2010. He was a postdoctor in University of Michigan (2010–2013), research associate in Brookhaven National Lab (2013–2014), research fellow and Japan Society for the Promotion of Science (JSPS) foreign fellow in University of Tokyo (2014–2015). He joined in Peking University in 2015. His research interests include electron microscopy, ferroelectrics, solid-state ionics, and structure and properties of crystal defects and interfaces.